DOI: 10.13009/EUCASS2022-6008
9TH EUROPEAN CONFERENCE FOR AERONAUTICS AND SPACE SCIENCES (EUCASS)

Starting procedure for space-based laser trackers to autonomously reach far distant targets by means of very narrow beams

GAMBI Jose M[1*]
[1] *Univ. Carlos III de Madrid, 28911 Leganes, Spain*
[*] gambi@math.uc3m.es
GARCIA DEL PINO Maria L[2]
[2] *I.E.S. Alpajes, 28300 Aranjuez, Spain, lgarciadelpino@educa.madrid.org*
MOSSER Jonathan[3]
[3] *Technische Universität Wien, 1040 Vienna, Austria, jonathan.mosser@asc.tuwien.ac.at*
WEINMÜLLER Ewa B[4]
[4] *Technische Universität Wien, 1040 Vienna, Austria, ewa.weinmueller@tuwien.ac.at*

Abstract
In this work, we present the only starting procedure that allows space-based laser emitters to autonomously carry out accurate FSO transmissions to receivers in far distant trajectories by means of very narrow laser beams.

1. Introduction

This work is a continuation of the work presented in the 3AF-OPTRO Conference held in Versailles, in June 2022 [1]. We introduce an updated starting procedure for autonomous laser tracking that can be used when the target, *D*, follows a trajectory that is far distant to the trajectory of the tracker, *S*, as in some FSO transmissions. (These scenarios are so frequent that from now on we will regard *S* as the emitter and *D* as the receiver.)
We assume, as in [1], that *S* is capable of reaching *D* with very narrow laser beams, but also, unlike in [1], that there is no guarantee that *S* can accurately reach *D* with these beams due to the large distance between the trajectories of *S* and *D*. In these scenarios only a small number of emission directions can coincide with the LOS directions from *S* to *D*, which is the condition for *S* to autonomously carry out secure transmissions to *D* [2]. This is due to the difference of orbital speeds. Hence, from the operative standpoint autonomy can only be achieved if, after acquiring *D* by a wide laser beam, *S* is able to record the instants, if any, at which the observed transverse motion of *D* is zero (within a given tolerance.)
We arrive at the conclusion that the confidence in long-distant transmissions can only rely on the quality of the clocks and pointing instruments on board the emitters (see e.g. [3,4].) In fact, these instruments must be accurate enough for *S* to account for the post-Newtonian (p-N) corrections to the relative motion of *D* with respect to *S* all along the transmission (this has already been suggested in other contexts, see e.g. [5-7].)
The reason is that, together with the navigation systems, these instruments are essential parts of the systems with which the emission and reception instants are recorded by *S*, for it to compute the p-N corrections according to the structure suggested in [8]. These corrections are computed in real time, once the narrow laser beams initially emitted to *D* return from *D*, using the p-N tracking formula in [9], together with the relative p-N equations of *D* with respect to *S* introduced here.
In this context, we stress that the p-N corrections derived here, both with these formulae and equations, show that including them in the considered scenarios is essential for *S* to accurately compute the point-ahead angles from the LOS directions in order to reach *D*. In fact, according to [10] both formulae and equations account for the gravitational gradient along the trajectories of the laser beams emitted from *S* to *D*, and vice versa. Furthermore, these new equations account for the different behavior of the clocks on board of *S* and *D* as in the usual procedures already implemented for accurate space navigation and geolocation.
Finally, we note that these equations coincide with the equations in [1] in case the trajectories of *S* and *D* become close, so that the difference in the respective p-N corrections to the current Newtonian (N) predictions are of higher order.

DOI: 10.13009/EUCASS2022-6008

Hence, the equations introduced here can be part of the general procedure presented in [2] in case of long distant actions.

2. Previous considerations and results

The purpose of this work is twofold: first, to determine the orbital characteristics of those LEO laser emitters, *S*, that can autonomously send information to a GEO satellite, *D*, by means of very narrow laser beams, and second, to determine the instants at which *S* can start the emissions.
We now recapitulate previous results and considerations related to this work:
1. Autonomous LEO space-based laser trackers, *S*, able to perform shooting actions on LEO targets, *D*, can be very useful to help throw *D* into the atmosphere by means of ablations [1].
2. In scenarios where the relative velocity of *D* with respect to *S* is large, as it is the case here, the LOS and pointing directions to *D* are usually not the same [11]. In fact, for actions carried out with very narrow laser beams, they have to be considered different. Hence, there is only one procedure for *S* to autonomously start tracking *D* in LEO-GEO FSO transmissions [1].
3. According to the N geometric structure of the space around the Earth, in order to autonomously track *D*, *S* has to start the transmissions when the transverse component of the velocity of *D* as measured by *S* is zero [1]. These instants, if any, have to be recorded by the standard clocks on board *S*.
4. If the relative velocity of *D* with respect to *S* is large, each emission action requires the previous computation of the point-ahead angle to accurately determine the pointing direction to *D* [1]. This allows, in turn, to derive by laser tracking the range from *S* to *D*. Hence, the tracking procedures have to use the p-N formulae in [9].
5. As a consequence, the only instant where the pointing direction doesn't need be determined, is when the transverse velocity of *D* with respect to *S* is zero. In this case it would coincide with the LOS direction to *D* [2].
6. Even with the most accurate pointing instruments available, the N tracking formula and the N relative equations of *D* with respect to *S* do not provide enough accuracy to prevent some undesirable effects, like spilling information around a distant *D*. This holds even after any standard perturbation has been included to model the motions of *S* and *D*. (An analysis of the issues related to FSO unmanned platform can be found in [12].)
7. Due to computational limitations and the instruments on board *S*, the emission and reception events can only be accurately determined within small time intervals. Nonetheless, they depend on the implementation of sequences of the p-N corrections to the standard point-ahead angles corresponding to the p-N description of the relative motion of *D* with respect to *S*.
8. Consequently, if these corrections are not taken into account all along the FSO transmissions it will eventually lead to significant errors according to the p-N formalism.

3. Autonomy for long-distant trajectories. Application to FSO transmissions

According to the p-N formalism, the tracking formula is universal [9], but the equations in [1] are not. In fact, the equations in [1] only yield accurate results when the trajectories of *S* and *D* are close, since in that case the recorded times can be assumed to be the same (see the first equation in (A1)). However, they are not suitable for *S* to reach receivers *D* in far-distant trajectories. That is why we adopt the equations in (2), see below.
The technical reason is that for *S* to accurately describe distant trajectories, the relative equations of *D* with respect to *S* must account for the different behavior of the clocks on board *S* and *D*, as for space navigation and geolocation. (Note that the roles of *S* and *D* are interchangeable.)
The p-N tracking formula reads:

$$R_{pN} = \frac{s' - s''}{2} \quad \left[1 - \frac{m}{2}\int_0^1 (1-u)^2 \left(\frac{3\left(\boldsymbol{R}_N \cdot \boldsymbol{r}_N(u)\right)^2}{r_N(u)^5} - \frac{\boldsymbol{R}_N^2}{r_N(u)^3}\right) du\right], \tag{1}$$

where s' and s'' are the emission and reception instants at *S* of a ranging beam sent to *D*, $\boldsymbol{R}_N$ is the Euclidean position of *D* with respect to S, and m is the mass of the Earth. This formula accounts for the gravitational gradient along the trajectories $\boldsymbol{r}_N(u)$ of the laser beams from *S* to *D*, and vice versa.
In turn, the p-N relative equations are, see Appendix A,

DOI: 10.13009/EUCASS2022-6008

$$\frac{d^2X_{(\alpha)}}{dt^2} = -m\left[X^{(\beta)}\int_0^1 (1-2u+3u^2)\left(\frac{3x_\alpha(u)x_\beta(u)}{r(u)^5}-\frac{\delta_{\alpha\beta}}{r(u)^3}\right)du + X^{(\beta)}X^{(\gamma)}\int_0^1 (1-u)u^2\frac{\partial}{\partial x^\alpha}\left(\frac{3x_\beta(u)x_\gamma(u)}{r(u)^5}-\frac{\delta_{\beta\gamma}}{r(u)^3}\right)du,\right]\cdot\left(1-\frac{2m}{r_D}-v_D^2\right) + \frac{2m}{r_S^3}\left(1+\frac{2m}{r_S}\right)\left(x_S^\gamma\frac{dx_S^\gamma}{dt}\right)\frac{dX_{(\alpha)}}{dt}, \quad (2)$$

where $X_{(\alpha)}$ are the p-N relative coordinates of *D* with respect to *S*, so that (x_S^γ, r_S) and (x_D^γ, r_D) are the ECI Euclidean positions and distances of *S* and *D*. The integrals are calculated along the straight-line that joins *S* and *D*.
We note that, like in LEO-LEO scenarios, these equations account for the gravitational gradient from *S* to *D*. Moreover, they cannot be used when the LOS from *S* to *D* is hidden by the Earth. In this case *D* obviously cannot be tracked by *S*. Due to this physical constraint the line integrals in (2) (also in (1)) become divergent when the line joining *S* and *D* theoretically passes through the center of the Earth. Therefore, the equations in (2) have to be substituted by the difference of the ECI equations of *S* and *D*, see [13],

$$\frac{d^2x^\alpha}{dt^2} = \frac{-mx^\alpha}{r^3}\left[1-\frac{2m}{r}+\left(2\delta_{\beta\gamma}-\frac{3x^\beta x^\gamma}{r^2}-\frac{2m}{r}\frac{x^\beta x^\gamma}{r^2}\right)\frac{dx^\beta}{dt}\frac{dx^\gamma}{dt}\right] + \frac{2m}{r^3}\left(1+\frac{2m}{r}\right)\left(x^\gamma\frac{dx^\gamma}{dt}\right)\frac{dx^\alpha}{dt}. \quad (3)$$

We also note, that while dealing with the integrals in (2), we have some freedom in choosing the instants to match the solutions of the equations (2) and (3). In fact, these instants depend on the orbital eccentricity of *S* and on the altitude of the atmosphere. Therefore, the way how equation (2) is replaced by equation (3) finally depends on the quality of the *S*-*D* transmissions.

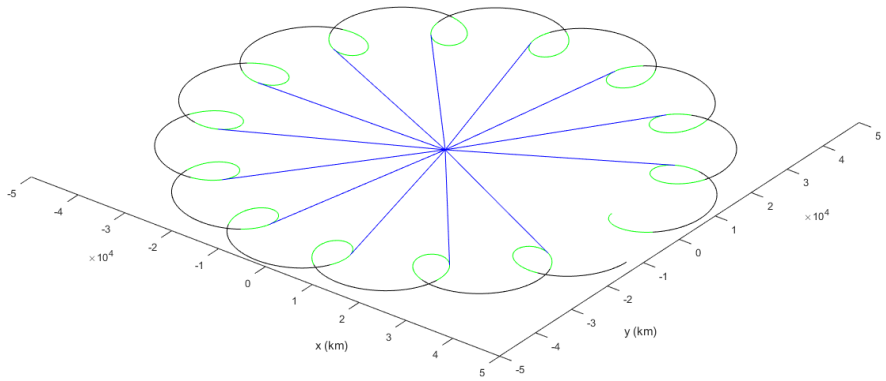

Figure 1: Relative orbit of *D* w.r.t. *S* (LOS-green, eclipse-black) and initial instants of autonomy (blue straight lines)

Fig. 1 shows the relative motion of a GEO satellite, *D*, with respect to a slightly eccentric emitter, *S* ($e = 0.01$) in equatorial orbit during (almost) one day. The orbital data of *S* are rather common, since its altitude at perigee is 460 km above the Earth surface, and the atmosphere is quite permeable. (The time span is 23 hours to facilitate the interpretation.)
In this figure the green (resp., black) paths correspond to the time intervals in which *D* is (resp., is not) in the LOS of *S*, so that *S* can start autonomous transmissions with very narrow beams within the green path of each epicycle of *D* with respect to *S*. This means that *S* can only perform the transmissions until the next eclipse (black) phase, where the autonomy is lost, according to the discussion above.
The blue straight lines correspond to the instants at which *S* can start autonomous transmissions. They are the first of the two tangents to the green arcs in each epicycle, and correspond to the instants at which the tangent to the green path of *D* is in the direction *D*-*S* (i.e., when *D* is approaching *S*), so that the transverse component of the relative velocity of *D* with respect to *S* is zero (see also the discussion for Figs.4-5 that corresponds to this fact). These lines are also represented in Fig.2, which would correspond to a theoretical exterior ECI observer, where the red orbit corresponds to *S*, and the blue one, to *D* (the black straight line corresponds to the final LOS.)

DOI: 10.13009/EUCASS2022-6008

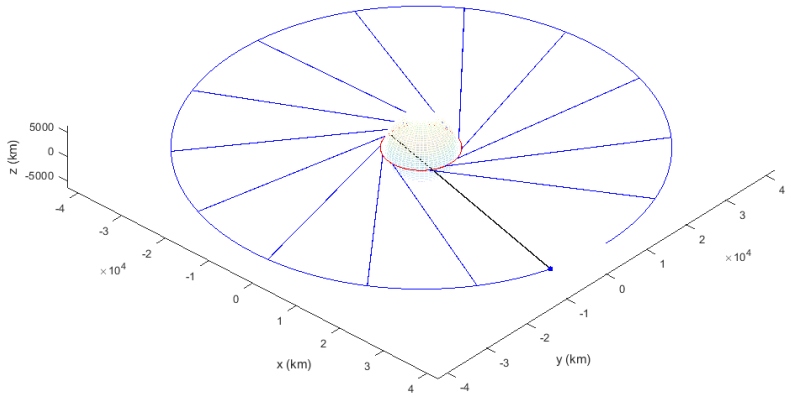

Figure 2: ECI orbits of *S* (red) and *D* (blue) and initial instants of autonomy (blue straight lines)

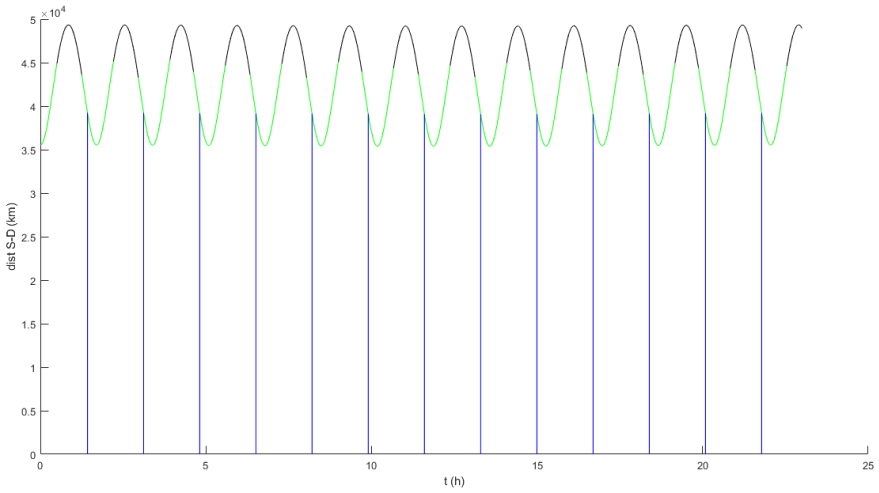

Figure 3: Relative distance of *D* w.r.t. *S* and initial instants of autonomy (blue straight lines)

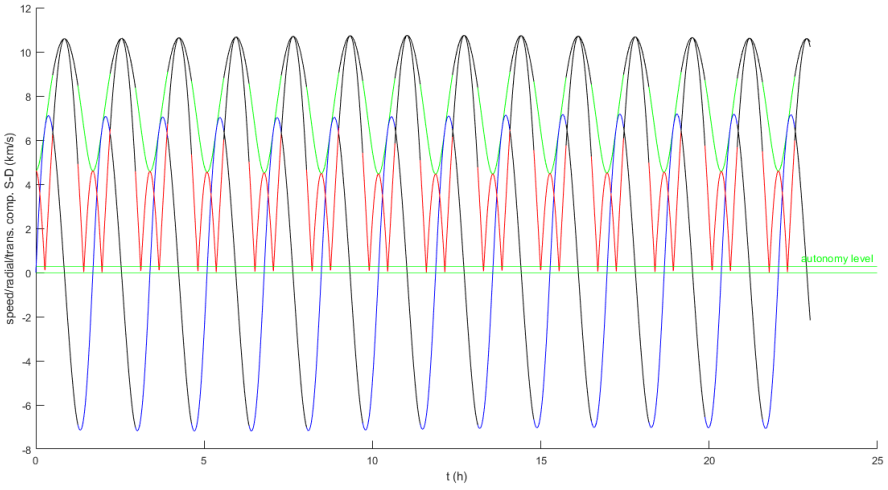

Figure 4: Relative velocity of *D* w.r.t. *S*: total speed (LOS-green, eclipsed-black) and radial (blue/black) and transverse (red/black) components. Tolerance level for autonomy line (green)

DOI: 10.13009/EUCASS2022-6008

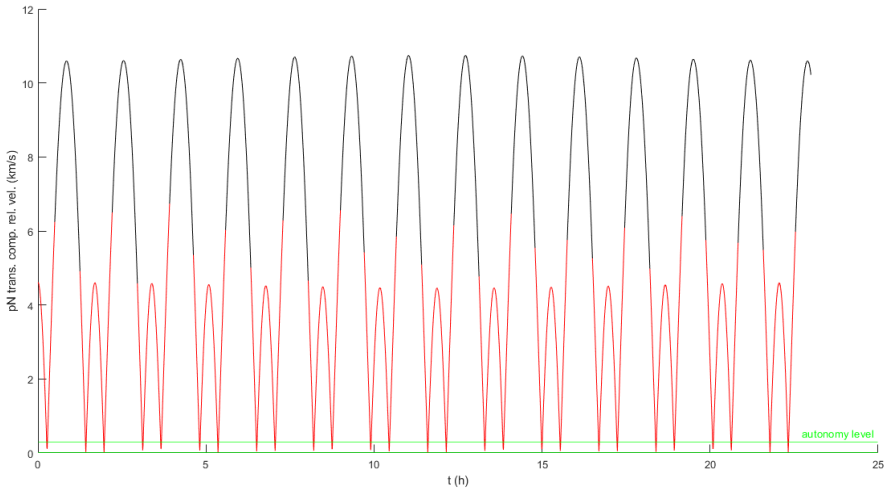

Figure 5: Transverse component of the relative velocity of *D* w.r.t. *S* (LOS-red, eclipsed-black). Tolerance level for autonomy line (green)

Fig. 3 shows the time evolution of the distance from *S* to *D*, with the same meaning for the green, black, and blue colors already given in Fig. 1. Note that the positions of the blue straight lines are in the descending green arcs.
Fig. 4 shows the time evolution of the total speed (green), and the radial (blue) and transverse (red) components of the velocity of *D* with respect to *S*, and Fig. 5 again shows the transverse component in detail, with the same meaning for the black arcs.
In latter two figures, the horizontal green lines represent the tolerance reflecting the limitations and potential inaccuracies of the instruments on board *S*. These lines are here enlarged. In practice, the tolerance must be small enough and previously fixed, taking into account the characteristics of the instruments on board. This implies that we must adopt the N magnitude of the time intervals that contain the starting autonomous instants.
We point out, that in this example, there are as many initial instants for *S* to become autonomous as there are epicycles in the relative trajectory of *D* with respect to *S*. This always applies when the orbit of *S* is coplanar with the orbit of *D*. The number of epicycles depends on the altitude of *S*. The higher the altitude, the fewer epicycles are in a given time span.

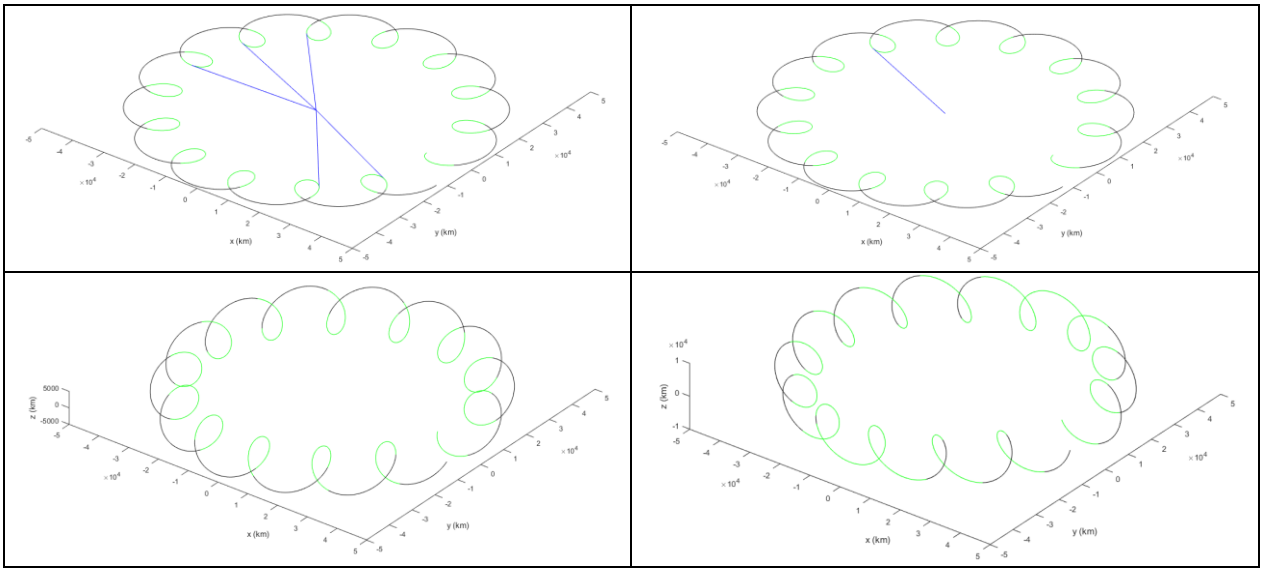

Figure 6: Sequence of relative orbits of *D* w.r.t. *S* and initial instants of autonomy

As the inclination of *S* increases, no matter the distance from S to *D*, the number of autonomous instants decreases drastically. It turns out, that the inclination of a LEO emitter, *S*, must be smaller than pi/150 rad, or 1.2º, to find at least one instant allowing *S* to become autonomous during one day.
Figs. 6-10 show the evolution of the number of instants as the inclination of *S* increases. The successive inclinations (from left to right) are $\pi/500$ rad ≡0.36º; $\pi/150$ rad ≡1.2º; $\pi/4$ rad ≡45º and $\pi/2$ rad ≡90º.

DOI: 10.13009/EUCASS2022-6008

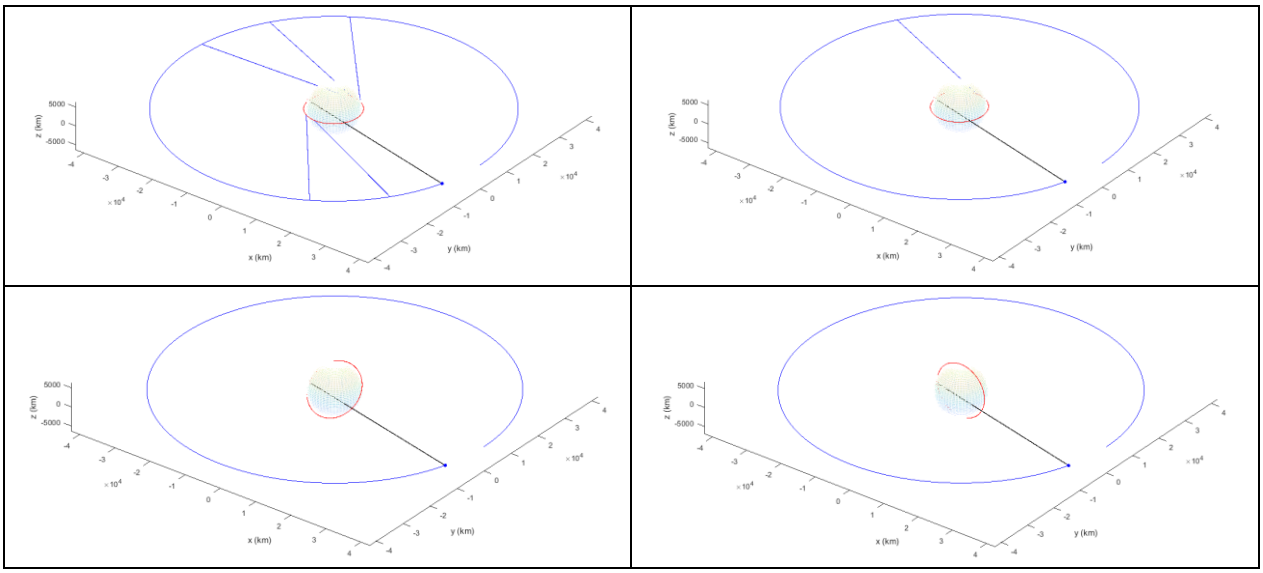

Figure 7: Sequence of ECI orbits of *S* and *D* and initial instants of autonomy

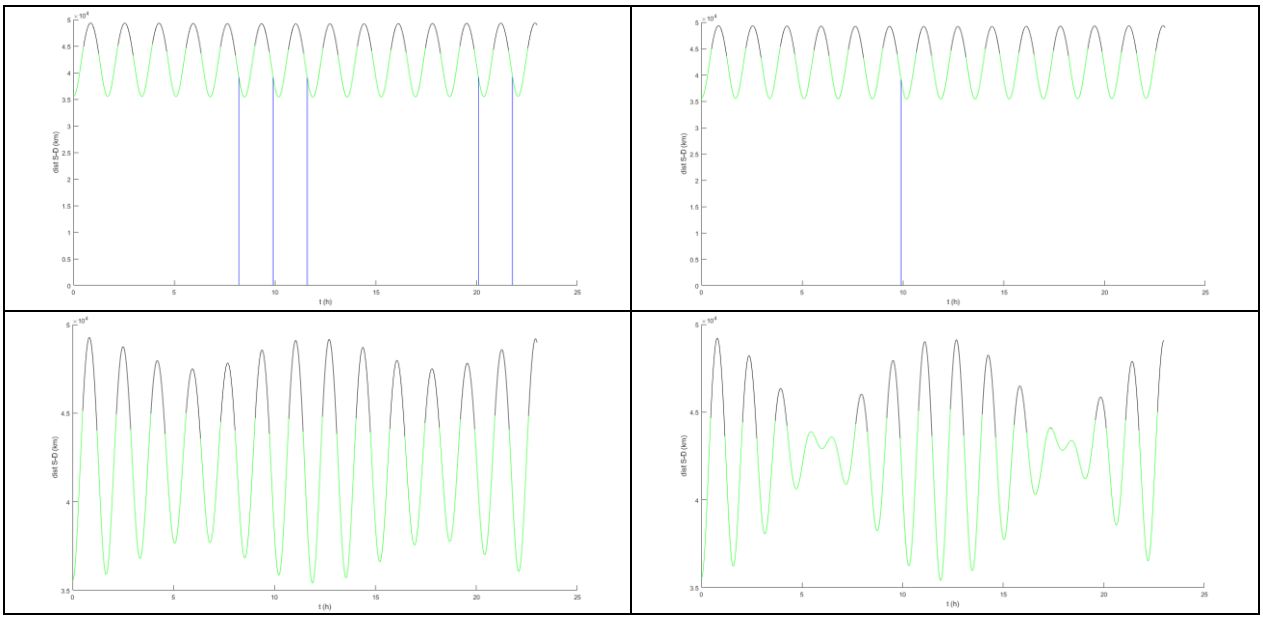

Figure 8: Sequence of relative distances of *D* w.r.t. *S* and initial instants of autonomy

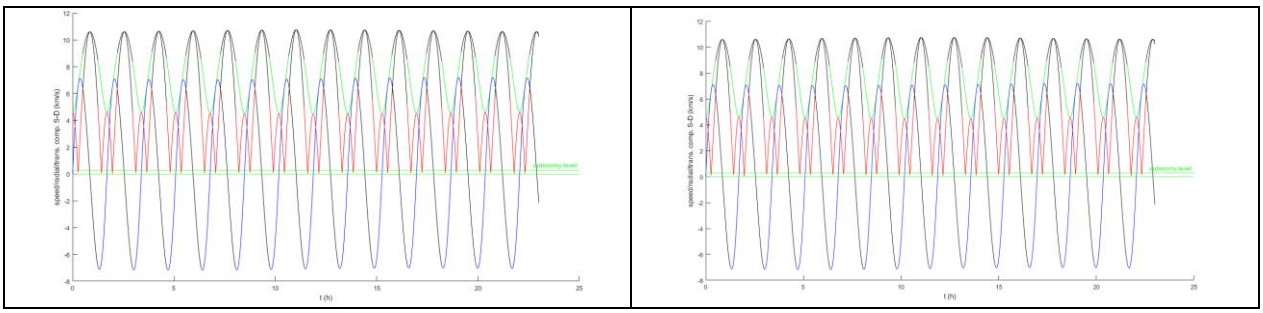

DOI: 10.13009/EUCASS2022-6008

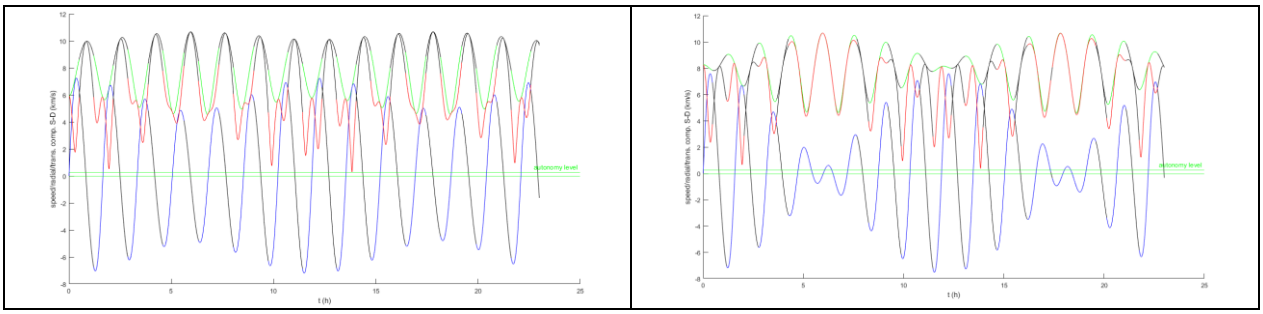

Figure 9: Sequence of relative velocities of *D* w.r.t. *S*: total speed and radial and transverse components with tolerance level for autonomy line

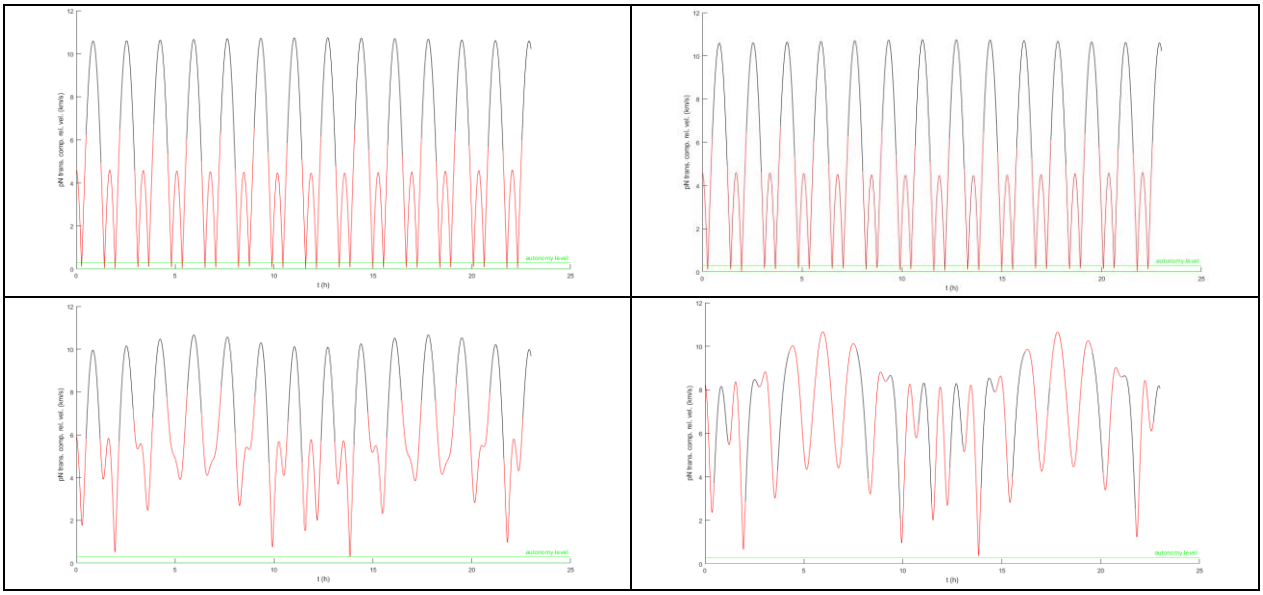

Figure 10: Sequence of transverse components of the relative velocities of *D* w.r.t. *S* with tolerance level for autonomy line

These sequences show the smooth evolution of the shape of the epicycles, and of the relative distances and velocities. In particular, they show how the transverse component of the relative velocity becomes too large in terms of permitted tolerances. (Note that the tolerance lines in Fig. 10 are also enlarged.)

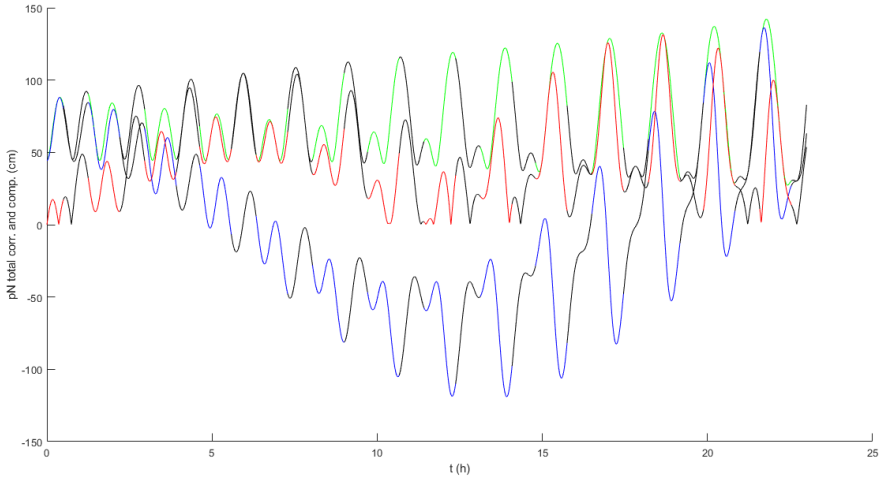

Figure 11: p-N corrections to the position of *D* w.r.t. *S*: total (LOS-green, eclipsed-black) and radial (blue/black) and transverse (red/black) components

DOI: 10.13009/EUCASS2022-6008

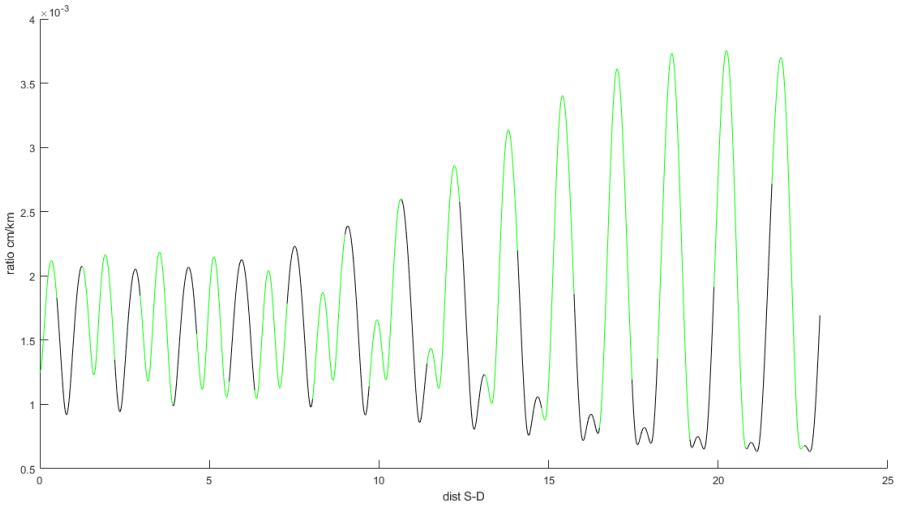

Figure 12: Ratio (cm/km) p-N corrections / rel. distance *S-D* (LOS-green, eclipsed-black)

In the case of $\pi/150$ rad ≡1.2º, the p-N corrections to the relative motion of *D* with respect to *S* should be considered all along the transmission to achieve secure emissions, especially during long time spans. Thus, for this slightly eccentric equatorial LEO emitter, altitude $\approx 460km$, the following p-N corrections and the ratio of these corrections to the distance *S-D* during one day can be found in Figs. 11 and 12, respectively.

Conclusion

The aim of this work is rather different than in [5], [6] and [7], where the goal was to increase shooting accuracy. Here the aim was to derive reasonable time intervals for *S* to autonomously start long-distance emissions. This means in practice, to find time intervals for which the transverse component of the velocity of *D* with respect to *S* is reasonably small, i.e., negligible. This implies that the relativistic corrections aimed at synchronizing the clocks of different LEO emitters are only to be taken into account to compute the p-N corrections derived from the equations in (2) (see e.g. [14].)
The main conclusion is that a time interval for any LEO emitter, to initiate autonomous FSO transmission to a GEO satellite, cannot always be found. In fact, for those emitters which can autonomously perform transmissions, the orbital inclination has to be as close to zero as possible, that is to say, in practice, not larger than $\pi/150$ rad ≡1.2º.

Appendix A

The procedure to arrive at the equations in (2) is a bit more general than the one in [6]. We start with the simplest, i.e., the current description of the components of the INS on board of *S*, $\lambda^i_{(\alpha)}$, and with the local metric, g_{ij}, around *S*, namely (Latin indices run from 1 to 4, and Greek, from 1 to 3),

$$\lambda^4_{(4)}\left(x^i_S\right) = (ds_S/dt)^{-1} = 1 + \frac{m}{r_S} + \frac{1}{2}(v_S)^2 + O(\varepsilon^4),$$

$$\lambda^\alpha_{(4)}\left(x^i_S\right) = \lambda^4_{(\alpha)} = v^\alpha_S + O(\varepsilon^3),$$

$$\lambda^\beta_{(\alpha)}\left(x^i_S\right) = \delta^\beta_\alpha - \frac{m}{r_S}\frac{x^\alpha x^\beta}{r_S^2} + \frac{1}{2}v^\alpha_S v^\beta_S + O(\varepsilon^3), \qquad (A1)$$

and

$$g_{(\alpha\beta)}\left(x^i_D\right) = \delta_{\alpha\beta} + 3\sigma^{-3}X^{(\mu)}X^{(\nu)}\int_0^\sigma (\sigma - u)u\, S_{(\alpha\beta\mu\nu)}du + O(\varepsilon^3),$$

$$g_{(\alpha 4)}\left(x^i_D\right) = O(\varepsilon^3),$$

$$g_{(44)}\left(x^i_D\right) = -1 + 3\sigma^{-3}X^{(\mu)}X^{(\nu)}\int_0^\sigma \sigma(\sigma - u)\, S_{(44\mu\nu)}du + O(\varepsilon^3), \qquad (A2)$$

DOI: 10.13009/EUCASS2022-6008

where $X^{(\mu)}$ are the local coordinates of *D* with respect to *S*, $S_{(abcd)}$ is the projection of the symmetrized Riemann tensor about *S* on $\lambda^i_{(a)}$, and $\varepsilon^2 = O(m/r)$. Therefore,

$$S_{(abcd)} = S_{ijkl}\lambda^i_{(a)}\lambda^j_{(b)}\lambda^k_{(c)}\lambda^l_{(d)},$$

so that

$$R_{(abcd)} \equiv -\big(S_{(acbd)} - S_{(adbc)}\big),$$

with

$$R_{(\alpha 4\gamma 4)} = -m\left(\frac{3x_\alpha x_\gamma}{r^5} - \frac{\delta_{\alpha\gamma}}{r^3}\right), \tag{A3}$$

where *m* is the mass of the Earth (measured in seconds), $r^2 = x_\alpha x^\alpha$ and x^α are ECI coordinates.
In terms of the world-function that joins two arbitrary events P_S and P_D of *S* and *D*,

$$\Omega(P_S, P_D) = \frac{1}{2}\int_{P_S}^{P_D} g_{ij}\frac{dx^i}{du}\frac{dx^j}{du},$$

the equations for the relative motion of *D* with respect to *S*, when P_S and P_D are simultaneous with respect to *S*, read:

$$\frac{d^2X_{(\alpha)}}{ds_S^2} = -\Omega_{(\alpha 44)} - 2\Omega_{(\alpha 44\prime)}\frac{ds_D}{ds_S} - \Omega_{(\alpha 4\prime 4\prime)}\left(\frac{ds_D}{ds_S}\right)^2, \tag{A4}$$

where

$$\Omega_{(\alpha 44)} = -X_D^\gamma\int_0^1 (1-u)^2\, R_{(\alpha 4\gamma 4)}du,$$

$$\Omega_{(\alpha 44\prime)} = X_D^\gamma\int_0^1 (1-u)^2\, R_{(\alpha 4\gamma 4)}du,$$

$$\Omega_{(\alpha 4\prime 4\prime)} = 2X_D^\gamma\int_0^1 u^2\, R_{(\alpha 4\gamma 4)}du - X_D^\mu X_D^\nu\int_0^1 (1-u)u^2\frac{\partial R_{(\mu 4\nu 4)}}{\partial x^\alpha}du$$

and

$$\frac{ds_D}{ds_S} = 1 + \frac{m}{r_S} - \frac{m}{r_D} + \frac{1}{2}v_S^2 - \frac{1}{2}v_D^2. \tag{A5}$$

Then, from the first equations in (A1), (A3), (A4), and (A5), we finally arrive at the equations in (2).

References

[1] Gambi, J. M., Garcia del Pino, M. L., Mosser, J., and Weinmüller, E.B. Starting procedure for LEO trackers to autonomously shoot at reflecting targets in close trajectories using very narrow laser beams. paper 80-212, 2022. *10th Int. Symp. on Optronics in Defense and Security, 3AF OPTRO2022*. Versailles, France.

[2] Gambi, J.M. and Garcia del Pino, M.L. Autonomous shooting at middle size space debris objects from space-based APT laser systems. 2017. Acta Astro **131**, 83-91, doi10.1016/j.actaastro.2016.11.026.

[3] Bandera, P A fine pointing mechanism for intersatellite laser communication. 1999. *European Space Agency-Publications-ESA SP* **438**, 61-66.

DOI: 10.13009/EUCASS2022-6008

[4] Hemani, K., Jain, V.K. and Subrat, K., Free Space Optical Communication. 2017. Springer, New Delhi. doi:10.1007/978-81-322-3691-7.

[5] Gambi, J.M., Garcia del Pino, M.L., Mosser, J. and Weinmüller, E.B. Computational modeling and simulation to increase laser shooting accuracy of autonomous LEO trackers. 2021. Photonics, **8**, pp. 55-61. doi:10.3390/photonics8020055

[6] Gambi, J.M., Garcia del Pino, M.L., Mosser, J and Weinmüller, E.B. Computational Procedure to increase the shooting accuracy of swarms of space-based laser trackers to deflect NEOS by means of ablation. 2021. 7th IAA Planetary Defense Conference. April 2021. Vienna, Austria.

[7] Gambi, J.M., Garcia del Pino, M.L., Mosser, J and Weinmüller, E.B. Trailing formations of lightweight spacecrafts to deflect NEAs by means of laser ablation. 2022. *Acta Astronautica*, **190**, pp. 241-250. doi: 10.1016/j.actaastro.2021.10.006.

[8] Landau, L.D and Lifshitz E.M., The Classical Theory of Fields. 1975. Elsevier BV: Amsterdam, The Netherlands. pp. 378–379.

[9] Gambi, J.M. and García del Pino, M.L. Post-Newtonian tracking formulae to increase the shooting accuracy of autonomous LEO laser trackers. 2021. Adv. Space Res. 67 2282–2303, http://dx.doi.org/10.1016/j.asr.2021.01.028.

[10] Synge, J.L. The World-function. In Relativity: The General Theory, Ch.2. 1960. Nord Holland: New York, NY, USA.

[11] Leeb, W R. Laser Space Communications: Systems, Technologies, and Applications 2000. *Rev. of Laser Engineering*, 28, 12, pp. 804–808, and *http://publik.tuwien.ac.at/files/pub.at4235.pdf*.

[12] Majumdar, A.K. Advanced Free Space Optics (FSO). A Systems Approach. 2015. Springer, NY, Heidelberg, Dordrecht, London. ISSN 0342-4111. DOI 10.1007/978-1-4939-0918-6.

[13] Gambi, J.M., Batista, D.J. and Garcia del Pino, M.L. 2020. IEEE Tran. Aerospace and Elec. Systems, **56**, 4, pp. 3063-3079.

[14] Dassié, M. and Giorgi, G. Relativistic Modelling for Accurate Time Transfer via Optical Intersatellite Links. 2021. Aerotec. Missili Spaz. **100**, pp. 277-288. https://doi.org/10.1007/s42496-021-00087-1.